



# 2D Bi<sub>2</sub>O<sub>2</sub>Se Nanosheets for Non-Enzymatic Electrochemical Detection of H<sub>2</sub>O<sub>2</sub>

Basant Chitara, Tej B. Limbu, Jason D. Orlando, Kizhanipuram Vinodgopal, and Fei Yan\* Department of Chemistry and Biochemistry, North Carolina Central University, Durham, NC 27707, USA

Received 3 June 2020, revised \*\*\*\*\*\*, accepted \*\*\*\*\*\*, published \*\*\*\*\*\*, current version \*\*\*\*\*. (Dates will be inserted by IEEE; "published" is the date the accepted preprint is posted on IEEE Xplore®; "current version" is the date the typeset version is posted on Xplore®).

**Abstract**— Bismuth oxyselenide ( $Bi_2O_2Se$ ) has recently emerged as a promising 2D material for high-performance electronic and optoelectronic applications. However, its true potential is yet to be explored for chemical sensing applications. The present investigation highlights the first demonstration of a  $Bi_2O_2Se$  nanosheets-based sensor for nonenzymatic electrochemical detection of hydrogen peroxide ( $H_2O_2$ ). A solution-phase method is employed to synthesize  $Bi_2O_2Se$  nanosheets. Cyclic voltammetry is performed to study the quantitative detection of  $H_2O_2$  with a reduction potential of -0.68 V vs. Ag/AgCl in nitrogen-saturated 0.1 M PBS (pH 7.4). The  $Bi_2O_2Se$  nanosheets-based  $H_2O_2$  sensor shows efficient detection of  $H_2O_2$  in the range of 50 - 500  $\mu$ M with a sensitivity of 100  $\mu$ A mA<sup>-1</sup> cm<sup>-2</sup>, and negligible interference was observed for most of the common interferents such as NaCl, ascorbic acid, uric acid and dopamine. Furthermore, the applicability of this electrochemical approach for practical applications is confirmed by the observation of concentration-dependent effect of  $H_2O_2$  on the reduction current in artificial sweat, making  $Bi_2O_2Se$  nanosheets a compelling electrocatalyst candidate for the development of new wearable glucose sensors.

Index Terms—Sensor materials, catalysis, H<sub>2</sub>O<sub>2</sub> detection, selectivity, artificial sweat.

#### INTRODUCTION

Fast and accurate detection of hydrogen peroxide (H<sub>2</sub>O<sub>2</sub>) is highly desirable in bioimaging, healthcare, environmental analysis and explosive detection. A variety of techniques such as fluorometry, spectrophotometry, cell imaging, and electrochemical methods have been utilized for such applications, among which electrochemical methods offer low cost, high selectivity and fast detection [1]. In electrochemical detection methods, enzyme-based electrochemical sensors show superior performance over non-enzymatic counterparts. However, the challenge of enzyme cost as well as the cumbersome immobilization process including susceptibility to temperature and pH impede their commercial applications [2]. Thus, the current approach is to explore new materials which can offer peroxidase-like activity for electrochemical sensors. Following this, several nanomaterials such as noble metal nanoparticles, transition metal oxide nanostructures and carbon-based materials have been exploited for non-enzymatic detection of H<sub>2</sub>O<sub>2</sub> [2]. Currently, 2D materials such as graphene and its analogues exhibiting excellent electrocatalytic properties are also being explored for the non-enzymatic detection of H<sub>2</sub>O<sub>2</sub> [1]. Thus, it would be interesting to explore exotic 2D materials for electrochemical detection of H<sub>2</sub>O<sub>2</sub>.

 $Bi_2O_2Se$  owing to its extremely high carrier mobility (>20,000 cm<sup>2</sup>V<sup>-1</sup>s<sup>-1</sup> at 2 K), low effective mass (0.14 m<sub>0</sub>) and band gap

tunability, has already been exploited for electronic and optoelectronic applications [3], [4]. However, the true potential of this fascinating air-stable 2D Bi<sub>2</sub>O<sub>2</sub>Se is yet to be explored for chemical sensing applications. Bi<sub>2</sub>O<sub>2</sub>Se with tetragonal crystal structure belongs to space group symmetry I4/mmm (a = b = 3.88 Å, and c = 12.16 Å) [3]. The strongly bonded [Bi<sub>2</sub>O<sub>2</sub>]<sub>n</sub><sup>2n+</sup> and [Se]<sub>n</sub><sup>2n-</sup> layers are held together by weak electrostatic interactions in alternative manner giving rise to zipper 2D structure. Several methods have been utilized to synthesize ultrathin Bi<sub>2</sub>O<sub>2</sub>Se nanosheets such as chemical vapor deposition (CVD) [3], pulsed laser deposition [5], molecular beam epitaxy [6], and wafer-scale single crystalline Bi<sub>2</sub>O<sub>2</sub>Se films on SrTiO<sub>3</sub> and LaAlO<sub>3</sub> [7].

In the present investigation, a solution-based synthetic approach developed by Ghosh et al. [8] was modified to prepare  $Bi_2O_2Se$  nanosheets at room temperature. The catalytic activity of  $Bi_2O_2Se$  nanosheets showed a strong dependence on the concentration of  $H_2O_2$ , both in a PBS buffer (pH 7.4) solution and in an artificial sweat matrix.

This letter presents a unique application of  $Bi_2O_2Se$  nanosheets for nonenzymatic electrochemical detection of  $H_2O_2$  in artificial sweat. The rapid and low-cost synthesis of freestanding  $Bi_2O_2Se$  nanosheets with high yield can be readily employed for electrode applications in comparison to nanosheets grown over substrates. Although the  $\mu$ M-level sensitivity obtained from  $Bi_2O_2Se$  nanosheets appears to be much lower than that exhibited by other commercial  $H_2O_2$ 

electrochemical sensors, the sensor's dynamic range is sufficient for our intended application, i.e. the development of a wearable device for real-time monitoring of glucose in sweat.

#### II. EXPERIMENTAL

Bi<sub>2</sub>O<sub>2</sub>Se nanosheets were synthesized according to a previously reported method [8] with slight modifications. Specifically, a selenium powder was used as the Se source instead of selenourea [9]. Briefly, Bi(NO<sub>3</sub>)<sub>3</sub>.5H<sub>2</sub>O (100 mg) was added into a glass vial containing deionized water (20 mL) with continuous stirring. To this solution, a solution containing Se<sup>2</sup>-ions formed by the reaction of selenium powder (8 mg) with hydrazine hydrate (1 mL) was added while stirring. Further, ethylenediaminetetraacetic acid disodium salt (307 mg) was added to the solution. Thereafter, within 10 min a black solution was obtained upon the addition of KOH (120 mg) and NaOH (320 mg), indicating the formation of Bi<sub>2</sub>O<sub>2</sub>Se nanosheets. The final product was then collected by centrifugation and washed with deionized water several times, followed by filtration before drying at 80 °C overnight.

The X-ray diffraction data was collected using Panalytical X'Pert PRO MRD HR XRD System. HORIBA LabRAM Evolution RAMAN Microscope-Smart SPM Atomic Force Microscope was used to obtain AFM images of  $Bi_2O_2Se$  samples. The FEI Tecnai  $G^2$  Twin was employed for TEM imaging of  $Bi_2O_2Se$  nanosheets.

Electrochemical measurements were performed using a CV-50W Voltammetric Analyzer (Bioanalytical Systems, Inc.) All electrochemical measurements were carried out using a typical three-electrode system with a Pt wire counter electrode and an Ag/AgCl as the reference electrode.  $Bi_2O_2Se$  nanosheets (5 mg each) were dispersed in Nafion (1 mL) followed by sonication for 1 h. The working electrode was then fabricated by dropcasting the dispersion (10  $\mu L)$  of  $Bi_2O_2Se$  nanosheets over glassy carbon electrode (GCE). The cleaned GCE having Nafion® (10  $\mu L)$  was used as a control. Cyclic voltammetry was performed on the working electrode to obtain steady CV in  $N_2$  saturated PBS solution (pH 7.4). Thereafter, CV was recorded under different concentrations of  $H_2O_2$  at a scan rate of 100 mV/s. The amperometric response of the sensor was measured at -0.68 V to monitor the selectivity of the sensor.

## III. RESULTS AND DISCUSSION

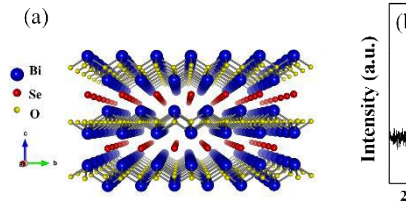
Eqs. 1-3 show the chemical reactions involved in the formation of  $Bi_2O_2Se$  nanosheets. In the first step,  $Bi(NO_3)_3$  undergoes hydrolysis to produce  $BiONO_3$ . In the second step, the element form of selenium is reduced by hydrazine to produce  $Se^{2-}$  in alkaline medium. In the third step, the self-assembly of oppositely charged  $(Bi_2O_2)^{2+}$  and  $Se^{2-}$  layers results in the formation of ultrathin  $Bi_2O_2Se$  nanosheets, which is subsequently separated as a black precipitate by centrifugation.

Bi(NO<sub>3</sub>)<sub>3</sub> + H<sub>2</sub>O 
$$\rightarrow$$
 BiONO<sub>3</sub> +2H<sup>+</sup> + 2NO<sub>3</sub><sup>-</sup> (1)

$$2Se + N_2H_4 + 4OH^- \rightarrow 2Se^{2-} + N_2 + 4H_2O$$
 (2)

$$2BiONO_3 + Se^{2-} \rightarrow Bi_2O_2Se + 2NO_3^-$$
 (3)

Fig. 1a illustrates the crystal structure  $Bi_2O_2Se$  having alternating stacks of  $[Bi_2O_2]_n^{2n+}$  and  $Se_n^{2n-}$  layers. Fig. 1b represents the XRD pattern of  $Bi_2O_2Se$  nanosheets. The broad XRD of the  $Bi_2O_2Se$  nanosheets is due to the ultrathin nature of  $Bi_2O_2Se$  nanosheets, however, these nanosheets exhibit a single crystalline nature as reported earlier [8].



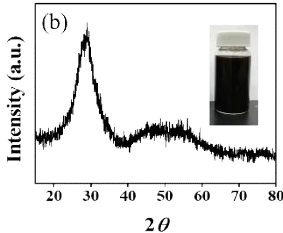
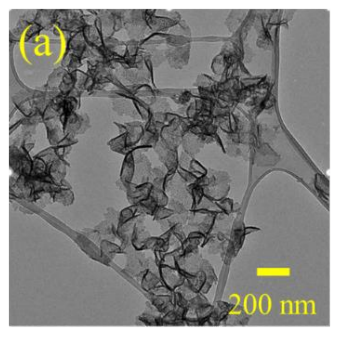


Fig. 1. (a) Schematic representation of crystal structure of  $Bi_2O_2Se$ . (b) XRD pattern of the  $Bi_2O_2Se$  nanosheets with  $Bi_2O_2Se$  nanosheets suspension in water shown as inset.

The morphology of the Bi<sub>2</sub>O<sub>2</sub>Se nanosheets is depicted in Fig. 2. Fig. 2a represents the TEM image of Bi<sub>2</sub>O<sub>2</sub>Se nanosheets. The AFM of the Bi<sub>2</sub>O<sub>2</sub>Se nanosheets with corresponding height profile (inset) has been presented in Fig. 2b. The thickness of the Bi<sub>2</sub>O<sub>2</sub>Se nanosheets was determined to be around 2-4 nm with a lateral dimension of 100-500 nm.



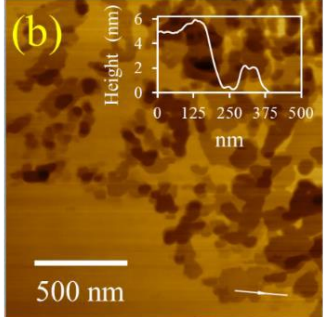


Fig. 2. (a) TEM image and (b) AFM image of Bi<sub>2</sub>O<sub>2</sub>Se nanosheets (with corresponding height profile shown as inset).

Fig. 3a displays the Raman spectrum of  $Bi_2O_2Se$  nanosheets with a characteristic  $A_{1g}$  peak at  $\approx 152$  cm<sup>-1</sup>.The UV-Vis-NIR spectrum of the  $Bi_2O_2Se$  nanosheets is shown as inset in Fig. 3a corresponding to bandgap of 1.5 eV [8]. Fig. 3b shows the CV of  $Bi_2O_2Se$  nanosheets with different concentrations of  $H_2O_2$  from 0 to 500  $\mu$ M. From the figure, it can be clearly seen that the oxidation peak current ( $I_{pa}$ ) and the reduction peak current ( $I_{pc}$ ) increase with an increasing concentration of  $H_2O_2$ . Since the reduction peak current is much higher than that of oxidation peak current and the interfering effect of common electroactive species is limited at negative applied potential, the reduction peak current at -0.68 V vs. Ag/AgCl was chosen for the determination of  $H_2O_2$ . The sensor shows an increase in

Article #

the cathodic peak current with a small shift of cathodic peak potentials upon the addition of  $H_2O_2$ , indicating the high catalytic activity of  $Bi_2O_2Se$  nanosheets for the reduction of  $H_2O_2$ , through electron transfer between the GCE and  $H_2O_2$ . The difference between the cathodic peak current for different  $H_2O_2$  concentration and the current without  $H_2O_2$  was used for the calibration curve. As shown as inset in Fig. 3b, the linear calibration curve I(µ)= -0.11C ( $H_2O_2$ ,  $\mu M$ ) – 8.5, corresponds to a sensitivity of 100  $\mu A$  mM-¹ cm-² for  $Bi_2O_2Se$  nanosheets in the range of 50 - 500  $\mu M$ . The performance of various 2D nonenzymatic  $H_2O_2$  sensors is presented in Table 1.

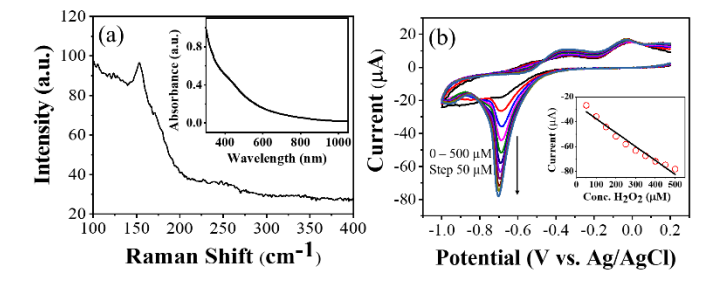


Fig. 3. (a) Raman spectrum of  $Bi_2O_2Se$  nanosheets with UV-Vis absorption spectrum shown as inset. (b) Cyclic voltammograms of a GCE modified with  $Bi_2O_2Se$  nanosheets with different concentrations of  $H_2O_2$  in  $N_2$ -saturated PBS solution (pH 7.4). Scan rate: 100 mV s<sup>-1</sup>. Inset: The linear regression to plots of the adjusted reduction current with the  $H_2O_2$  concentration. Each data represents the average of three measurements.

Table 1. Performance comparison of 2D materials based nonenzymatic H2O2 sensors

Material	Reduction Voltage vs. Ag/AgCl(V)	Sensitivity (µAmM <sup>-1</sup> cm <sup>-2</sup> )	Linear Range (µM)	Ref.
rGO/GCE	-0.20	82.35	0.05 - 1500	[9]
Cu <sub>2</sub> O- RGO/GCE	-0.30	19.5	30 - 12800	[10]
CdS nanorods- RGO/GCE	-0.83	95	5- 15000	[11]
O-MoS <sub>2</sub> - RGO	-0.34	269.7	250 - 16000	[12]
Ag NPs/MOS <sub>2</sub> /GCE	-0.54	54.5	25- 13500 0	[13]
MnO <sub>2</sub> - GO/GCE	-0.30	38.2	5 - 600	[14]
Au-MnO <sub>2</sub> - RGO/GCE	-0.2	980	0.1 - 22	[15]
Bi <sub>2</sub> O <sub>2</sub> Se	-0.68	100	50 - 500	This work

To further investigate the selectivity of  $Bi_2O_2Se$  nanosheets and examine its applicability for practical applications, the steady state amperometry was performed to detect  $H_2O_2$  in the presence of well-known interferents such as NaCl, ascorbic acid (AA), uric acid (UA) and dopamine (DA). As evident from Fig. 4, the addition of NaCl (0.2 mM), AA (0.2 mM), UA (0.2 mM) an DA (0.2 mM) does not cause a change in the cathodic peak current whereas the addition of  $H_2O_2$  (0.1 mM) show a significant change in the signal. Thus, the coexistence of interferents such as NaCl, AA, UA and DA does not affect the performance of the electrocatalytic activity of  $Bi_2O_2Se$  nanosheets.

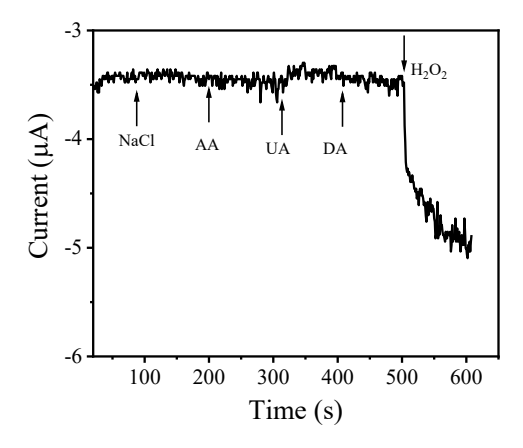


Fig. 4. Amperometric responses of the  $Bi_2O_2Se$  nanosheets to the addition of different analytes in 0.1 M PBS (pH = 7.0): 0.1 mM  $H_2O_2$ , 0.2 mM DA, 0.2 mM AA, 0.2 mM UA, and 0.2 mM NaCl at - 0.68 V.

For Bi<sub>2</sub>O<sub>2</sub>Se nanosheets to be utilized in future wearable sweat sensors [16], [17], we have tested the catalytic activity of Bi<sub>2</sub>O<sub>2</sub>Se nanosheets in artificial sweat. Artificial sweat with a pH of 8.0 was prepared as per the standard of the International Standard Organization (ISO105-E04-2008E) [18]. Briefly, Lhistidine monohydrochloride monohydrate 0.05 (w/v %), NaCl 0.50 (w/v %) and disodium hydrogen orthophosphate 0.20 (w/v %) were taken to achieve the desired artificial sweat (pH 8.0). Again, cyclic voltammetry was performed on the working electrode to obtain steady CV in N<sub>2</sub>-saturated artificial sweat (pH 8.0) under different concentrations of H<sub>2</sub>O<sub>2</sub> at a scan rate of 100 mV/s.

As shown in Fig. 5, in the absence of  $H_2O_2$ , the L-histidine in the artificial sweat showed electrochemical activity at pH 8.0 on  $Bi_2O_2Se$  nanosheets-coated GC electrode, as evidenced by the presence of a reduction peak potential at - 0.8 V vs. Ag/AgCl. This could result from the complexation between L-histidine and the residual metal ions (e.g.  $Bi^{3+}$  ions) on the modified electrode [19]. The sequential addition of  $H_2O_2$  led to an appearance of another reduction peak potential at - 0.62 V vs. Ag/AgCl, a slight shift from its original place at - 0.68 V vs. Ag/AgCl in 0.1 M PBS (pH 7.4), which could be explained by the pH effect on the reduction of  $H_2O_2$  [20]. There appears to

exist an "isosbestic point" at - 0.7 V vs. Ag/AgCl, suggesting that a displacement reaction might occur between L-histidine and  $H_2O_2$ . The cathodic current corresponding to the reduction peak potential at - 0.62 V vs. Ag/AgCl increases with the increasing concentration of  $H_2O_2$  in the range of 50-200  $\mu\text{M}$ , confirming the feasibility of detecting  $H_2O_2$  in a sweat matrix. Given that electrochemical  $H_2O_2$  sensing mechanism works exactly the same way for glucose detection, and the reported glucose level in sweat for healthy people is between 60  $\mu\text{M}$  and 110  $\mu\text{M}$  and between 10  $\mu\text{M}$  and 1000  $\mu\text{M}$  for diabetics [20], this study paves the way for the development of a wearable electrochemical sensor for real-time monitoring of glucose in sweat.

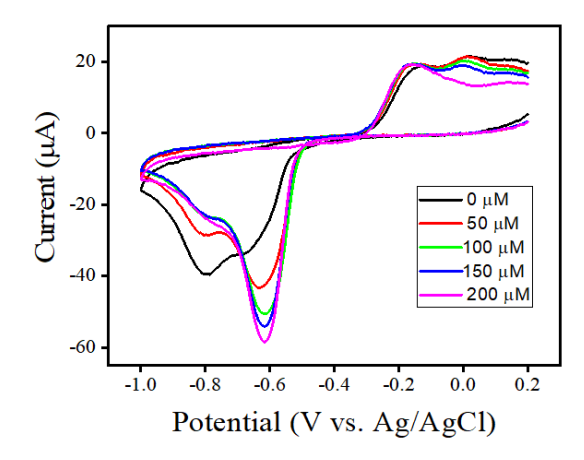


Fig. 5. Cyclic voltammograms of a GCE modified with  $Bi_2O_2Se$  nanosheets with different concentrations of  $H_2O_2$  in  $N_2$ -saturated artificial sweat (pH 8.0) at a scan rate of 100 mV s<sup>-1</sup>.

## IV. CONCLUSION

In summary, we demonstrated, for the first time, that  $Bi_2O_2Se$  nanosheets could serve as a robust electrocatalyst for non-enzymatic electrochemical detection of  $H_2O_2$ . The sensor shows efficient detection of  $H_2O_2$  in the range of 50 -  $500~\mu M$  with a sensitivity of  $100~\mu A~mA^{-1}~cm^{-2}$ . The electrode exhibits excellent selectivity for  $H_2O_2$  over common interferents including NaCl, AA, UA and dopamine. Moreover, the catalytic activity of  $Bi_2O_2Se$  nanosheets shows a strong dependence on the concentration of  $H_2O_2$  in an artificial sweat matrix, which makes them a promising electrocatalyst candidate for the development of a wearable device for real-time monitoring of glucose in sweat.

#### **ACKNOWLEDGMENT**

The authors are grateful for the financial support of this project by the U.S. National Science Foundation (Awards # 1831133 and #1523617). This work was performed in part at the Duke University Shared Materials Instrumentation Facility (SMIF), a member of the North Carolina Research Triangle Nanotechnology Network (RTNN), which is supported by the National Science Foundation (Grant ECCS-1542015) as part of the National Nanotechnology Coordinated Infrastructure (NNCI).

### REFERENCES

- [1] H. Shamkhalichenar and J.-W. Choi, "Review—Non-Enzymatic Hydrogen Peroxide Electrochemical Sensors Based on Reduced Graphene Oxide," J. Electrochem. Soc., vol. 167, no. 3, p. 037531, 2020.
- [2] C. Cheng, C. Zhang, X. Gao, Z. Zhuang, C. Du, and W. Chen, "3D Network and 2D Paper of Reduced Graphene Oxide/Cu2O Composite for Electrochemical Sensing of Hydrogen Peroxide," *Anal. Chem.*, vol. 90, no. 3, pp. 1983–1991,2018.
- [3] J. Wu et al., "High electron mobility and quantum oscillations in non-encapsulated ultrathin semiconducting Bi2O2Se," Nat. Nanotechnol., vol. 12, no. 6, pp. 530–534, 2017.
- [4] H. Yang et al., "Near-Infrared Photoelectric Properties of Multilayer Bi2O2Se Nanofilms," Nanoscale Res. Lett., vol. 14, no. 1, p. 371, 2019.
- [5] Y. Song et al., "Epitaxial growth and characterization of high quality Bi2O2Se thin films on SrTiO3 substrates by pulsed laser deposition," Nanotechnology, vol. 31, no. 16, p. 165704, 2020.
- [6] Y. Liang et al., "Molecular Beam Epitaxy and Electronic Structure of Atomically Thin Oxyselenide Films," Adv. Mater., vol. 31, no. 39, p. 1901964, 2019.
- [7] C. Tan et al., "Wafer-Scale Growth of Single-Crystal 2D Semiconductor on Perovskite Oxides for High-Performance Transistors," Nano Lett., vol. 19, no. 3, pp. 2148–2153, 2019.
- [8] T. Ghosh et al., "Ultrathin Free-Standing Nanosheets of Bi 2 O 2 Se: Room Temperature Ferroelectricity in Self-Assembled Charged Layered Heterostructure," Nano Lett., vol. 19, no. 8, pp. 5703–5709,2019.
- [9] M. Zhou, Y. Zhai, and S. Dong, "Electrochemical sensing and biosensing platform based on chemically reduced graphene oxide," *Anal. Chem.*, vol. 81, no. 14, pp. 5603–5613, 2009.
- [10] F. Xu, M. Deng, G. Li, S. Chen, and L. Wang, "Electrochemical behavior of cuprous oxide-reduced graphene oxide nanocomposites and their application in nonenzymatic hydrogen peroxide sensing," *Electrochimica Acta*, vol. 88, pp. 59–65, 2013.
- [11] X. An, X. Yu, J. C. Yu, and G. Zhang, "CdS nanorods/reduced graphene oxide nanocomposites for photocatalysis and electrochemical sensing," *J. Mater. Chem. A*, vol. 1, no. 16, pp. 5158–5164, 2013.
- [12] Y. Xue, G. Maduraiveeran, M. Wang, S. Zheng, Y. Zhang, and W. Jin, "Hierarchical oxygen-implanted MoS2 nanoparticle decorated graphene for the non-enzymatic electrochemical sensing of hydrogen peroxide in alkaline media," *Talanta*, vol. 176, pp. 397–405, 2018.
- [13] Z. Zhao et al., "Ag functionalized molybdenum disulfide hybrid nanostructures for selective and sensitive amperometric hydrogen peroxide detection," Int. J. Electrochem. Sci., vol. 12, no. 9, Art. no. 9, 2017.
- [14] L. Li et al., "A novel nonenzymatic hydrogen peroxide sensor based on MnO2/graphene oxide nanocomposite," *Talanta*, vol. 82, no. 5, pp. 1637– 1641, 2010.
- [15] Ii Wang, M. Deng, G. Ding, S. Chen, and F. Xu, "Manganese dioxide based ternary nanocomposite for catalytic reduction and nonenzymatic sensing of hydrogen peroxide," *Electrochimica Acta*, vol. 114, pp. 416– 423, 2013.
- [16] W. Gao et al., "Fully integrated wearable sensor arrays for multiplexed in situ perspiration analysis," Nature, vol. 529, no. 7587, Art. no. 7587, 2016.
- M. Bariya, H. Y. Y. Nyein, and A. Javey, "Wearable sweat sensors," Nat. Electron., vol. 1, no. 3, Art. no. 3, 2018.
- [18] K. Kulthong, S. Srisung, K. Boonpavanitchakul, W. Kangwansupamonkon, and R. Maniratanachote, "Determination of silver nanoparticle release from antibacterial fabrics into artificial sweat," Part. Fibre Toxicol., vol. 7, p. 8, 2010.
- [19] M. Medvidović-Kosanović, A. Stanković Ex Šter, M. Jozanović Horvat, M. Drulak, and M. Ilić, "Electrochemical and UV/VIS Study of L-Histidine and Its Complexes with Cobalt and Nickel," Croat. Chem. Acta, vol. 91,2018.
- [20] X. Xu, S. Liu, and H. Ju, "A Novel Hydrogen Peroxide Sensor via the Direct Electrochemistry of Horseradish Peroxidase Immobilized on Colloidal Gold Modified Screen-printed Electrode," Sensors, vol. 3, no. 9, Art. no. 9, 2003.